Materials and Structures/Matériaux et Constructions, 1989, **22**, 429–436

Snap-back softening instability in high-strength concrete beams

L. BIOLZI

Institute of Theoretical and Applied Mechanics, Universita di Udine, 33100 Udine, Italy

S. CANGIANO, G. TOGNON

ITALCEMENTI, 24100 Bergamo, Italy

A. CARPINTERI

Department of Structural Engineering, Politecnico di Torino, Corso Duca degli Abruzzi 24, 10129 Torino, Italy

Three-point bending tests on pre-cracked slabs of high-strength concrete are interpreted on the basis of a virtual crack propagation model. As theoretically shown by the model, a snap-back softening instability appears only for initial crack lengths smaller than 0.3 times the beam depth. As a limit-case, when the material is sufficiently brittle or the specimen size is sufficiently large, such an instability can be predicted by the LEFM condition $K_I = K_{IC}$.

1. INTRODUCTION

A theoretical and experimental investigation is carried out on the application of linear elastic fracture mechanics (LEFM) to high-strength concrete. The material is so brittle in this case that the size of the crack tip process zone is very small if compared with the size of the zone where the stress singularity field is dominant.

According to the model of virtual crack extension [1,2], the condition of stable crack growth is given by the LEFM condition $K_I = K_{IC}$ at each loading step. A snap-back phenomenon is predicted for large size-scales and for a short initial crack, as well as for brittle materials. The same trends have been found by Carpinteri [3] by using a non-linear cohesive crack model and by considering a cohesive limit analysis [4].

Pre-cracked three-point bend specimens of high-strength concrete are tested up to the complete load-relaxation and specimen separation. The load–deflection and load–crack mouth opening diagrams are regularly obtained without jumping and discontinuities. The loading process is controlled by a monotonically increasing function of time, i.e. the crack mouth opening displacement (CMOD). Even the virtual branch of catastrophical softening is clearly detected. While both load and deflection decrease along such a branch with positive slope, the crack opens and grows in a stable manner.

According to the prediction of the theoretical LEFM model, a snap-back instability appears experimentally only for initial crack lengths smaller than 0.3 times the beam depth. It is particularly interesting to verify that the bifurcation point is accurately described by the LEFM condition $K_I = K_{IC}$ for small initial cracks.

In this way, it is even experimentally proved that the LEFM instability is a limit case of the snap-back softening instability, when the material is sufficiently brittle, the specimen size is sufficiently large, and/or the crack length is sufficiently small. All the three material and geometrical conditions mentioned allow the stress singularity zone to develop and dominate.

2. APPLICATION OF DIMENSIONAL ANALYSIS

Due to the different physical dimensions of ultimate tensile strength, σ_u, and fracture toughness, K_{IC}, scale effects are always present in the usual fracture testing of common engineering materials. This means that, for the usual size-scale of the laboratory specimen, the ultimate strength collapse or the plastic collapse at the ligament tends to anticipate and obscure the brittle crack propagation. Such a competition between different types of collapse can easily be shown by considering the ASTM formula [5] for three-point bending test evaluation of fracture toughness (Fig. 1):

$$K_I = \frac{Pl}{tb^{3/2}} f\left(\frac{a}{b}\right) \tag{1}$$

with

$$f\left(\frac{a}{b}\right) = 2.9\left(\frac{a}{b}\right)^{1/2} - 4.6\left(\frac{a}{b}\right)^{3/2} + 21.8\left(\frac{a}{b}\right)^{5/2} - 37.6\left(\frac{a}{b}\right)^{7/2} + 38.7\left(\frac{a}{b}\right)^{9/2}$$

For crack propagation Equation 1 becomes

$$K_{IC} = \frac{P_{max} l}{tb^{3/2}} f\left(\frac{a}{b}\right) \tag{2}$$

where P_{max} is the external load of brittle fracture. If both sides of Equation 2 are divided by $\sigma_u b^{1/2}$ one obtains

$$\frac{K_{IC}}{\sigma_u b^{1/2}} = s = \frac{P_{max} l}{\sigma_u tb^2} f\left(\frac{a}{b}\right) \tag{3}$$

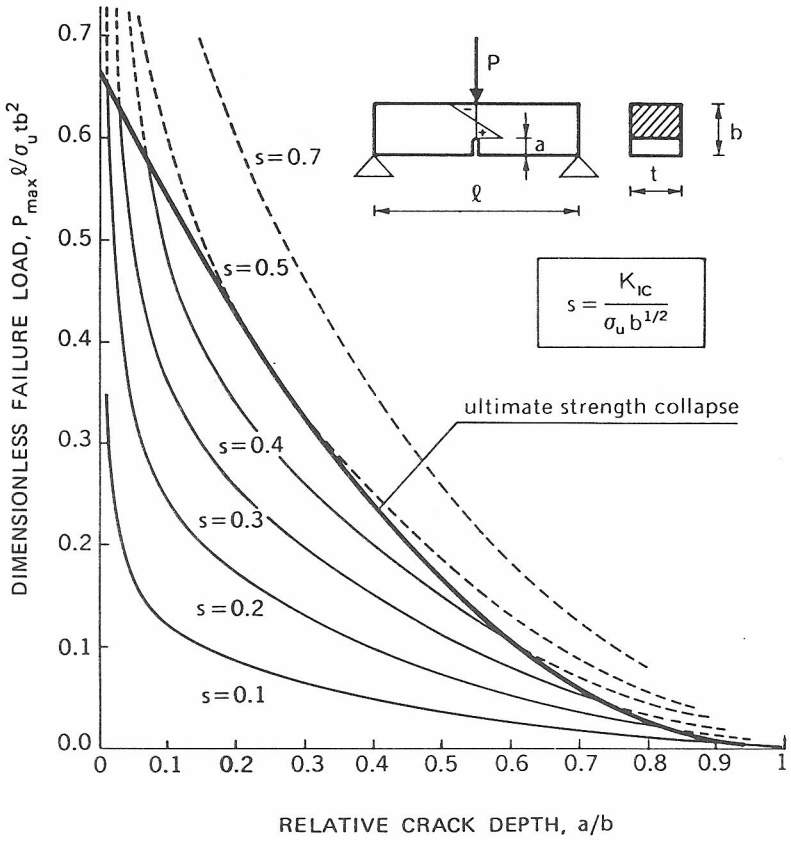

Fig. 1 Dimensionless load of crack instability against relative crack depth. $s = K_{IC}/\sigma_u b^{1/2}$.

where s is a dimensionless number able to describe the brittleness of the specimen [6,7]. Rearrangement of Equation 3 gives

$$\frac{P_{max} l}{\sigma_u tb^2} = \frac{s}{f(a/b)} \tag{4}$$

On the other hand, it is possible to consider the non-dimensional load of ultimate strength in a beam of depth $(b - a)$:

$$\frac{P_{max} l}{\sigma_u tb^2} = \frac{2}{3}\left(1 - \frac{a}{b}\right)^2 \tag{5}$$

Equations 4 and 5 are plotted in Fig. 1 as functions of the crack depth a/b. While the former produces a set of curves by varying the brittleness number s, the latter is represented by a unique curve. It is evident that the ultimate strength collapse at the ligament precedes crack propagation for each initial crack depth, when the brittleness number s is higher than the limit-value $s_0 = 0.50$. For lower s numbers, the ultimate strength collapse anticipates crack propagation only for crack depths external to a certain interval. This means that a true LEFM collapse only occurs for comparatively low fracture toughnesses, high tensile strengths and/or large structure sizes. It is not the single values of K_{IC}, σ_u and b that determine the nature of the collapse but only their function s (see Equation 3).

3. VIRTUAL PROPAGATION OF A BRITTLE FRACTURE

The flexural behaviour of the beam in Fig. 1 will now be analysed. The deflection due to the elastic compliance of the uncracked beam is

$$\delta_e = \frac{Pl^3}{48\,EI} \tag{6}$$

where I is the inertial moment. However, the deflection due to the local crack compliance is [8]

$$\delta_c = \frac{3}{2}\frac{Pl^2}{tb^2 E}\, g\left(\frac{a}{b}\right) \tag{7}$$

with

$$g\left(\frac{a}{b}\right) = \left(\frac{a/b}{1-(a/b)}\right)^2 \left[5.58 - 19.57\left(\frac{a}{b}\right) + 36.82\left(\frac{a}{b}\right)^2 - 34.93\left(\frac{a}{b}\right)^3 + 12.77\left(\frac{a}{b}\right)^4\right] \tag{8}$$

The superposition principle provides

$$\delta = \delta_e + \delta_c$$

and, in a non-dimensional form,

$$\frac{\delta l}{\varepsilon_u b^2} = \frac{Pl}{\sigma_u t b^2}\left[\frac{1}{4}\left(\frac{l}{b}\right)^3 + \frac{3}{2}\left(\frac{l}{b}\right)^2 g\left(\frac{a}{b}\right)\right] \quad (9)$$

where $\varepsilon_u = \sigma_u/E$. The term within square brackets is the dimensionless compliance, which turns out to be a function of the beam slenderness, l/b, as well as of the crack depth, a/b. Some linear load–deflection diagrams are represented in Fig. 2, by varying the crack depth a/b and for the fixed ratio $l/b = 4$.

Through Equations 4 and 5, it is possible to determine the point of crack propagation as well as the point of ultimate strength on each linear plot in Fig. 2. Whereas the former depends on the brittleness number s, the latter is unique. The set of the crack propagation points with s = constant and varying crack depth represents a virtual load–deflection path, where point by point the load is always that producing the crack instability [9].

When the crack grows, the load of instability decreases and the compliance increases, so that the product on the right-hand side of Equation 9 may either decrease or increase. The diagrams in Fig. 2 show the deflection first decreasing (with the load) up to the crack depth $a/b \simeq 0.3$ and then increasing (in opposition to the load). Therefore, whereas for $a/b \geqslant 0.3$ the P–δ curve presents the usual softening course with a negative derivative, for $a/b \leqslant 0.3$ it presents a positive derivative. Such a branch could not be observed by deflection-controlled testing and the representative point would jump from the positive to the negative branch with a behaviour discontinuity.

The set of ultimate strength points, for varying crack depth, is represented by the thick line in Fig. 2. Such a line intersects the virtual crack propagation curves for $s \leqslant s_0 = 0.50$, analogously to what is shown in Fig. 1, and depicts a slight indentation ($dP/d\delta > 0$).

The CMOD (w_1) is a function of the specimen geometry and of the elastic modulus [8]:

$$w_1 = \frac{6Pla}{tb^2E} h\left(\frac{a}{b}\right) \quad (10)$$

with

$$h\left(\frac{a}{b}\right) = 0.76 - 2.28\left(\frac{a}{b}\right) + 3.87\left(\frac{a}{b}\right)^2 - 2.04\left(\frac{a}{b}\right)^3 + \frac{0.66}{[1-(a/b)]^2} \quad (11)$$

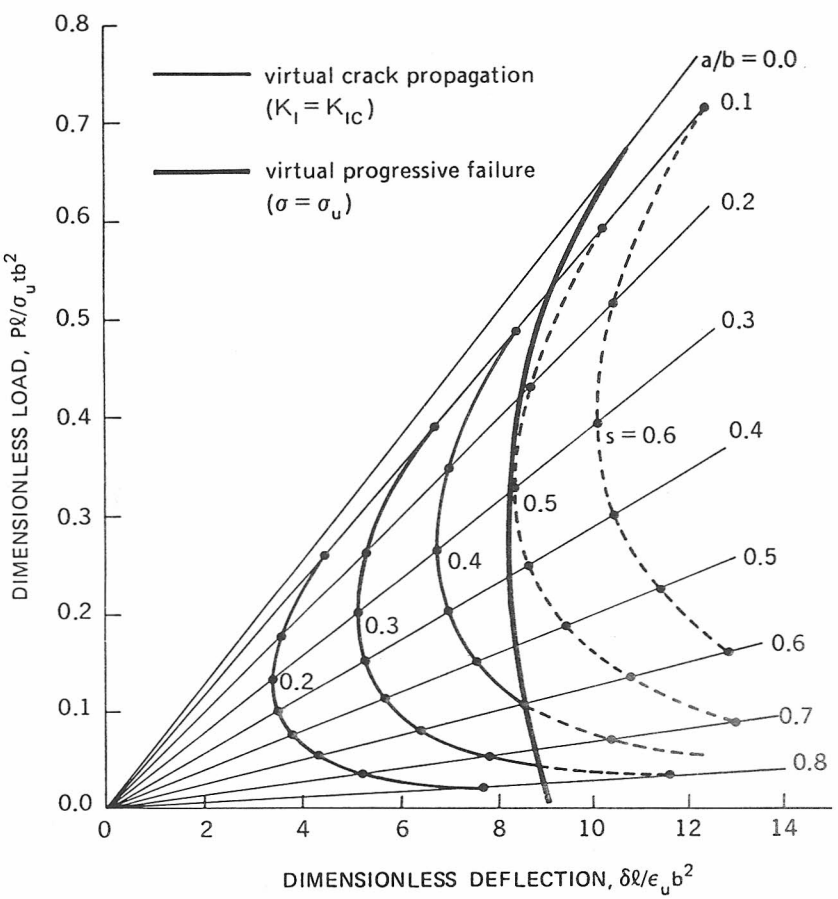

Fig. 2 Dimensionless load of crack instability against dimensionless deflection. (——) Virtual crack propagation ($K_I = K_{IC}$), (▬) virtual progressive failure ($\sigma = \sigma_u$).

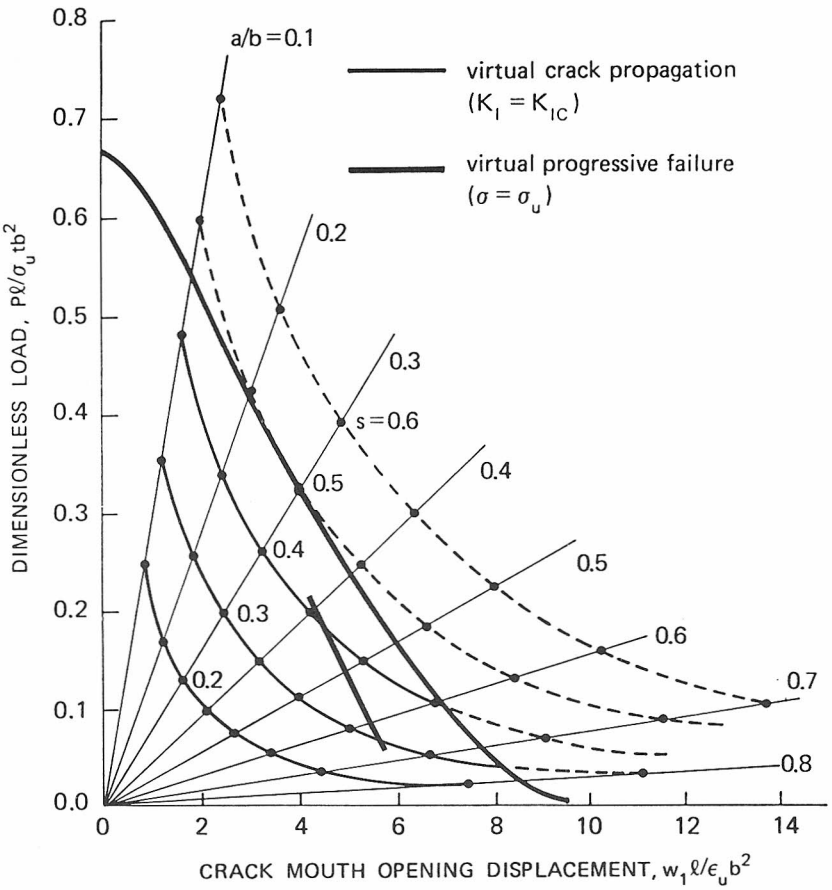

Fig. 3 Dimensionless load of crack instability against dimensionless crack mouth opening displacement. (——) Virtual crack propagation ($K_I = K_{IC}$), (▬) virtual progressive failure ($\sigma = \sigma_u$).

In a non-dimensional form Equation 10 becomes

$$\frac{w_1 l}{\varepsilon_u b^2} = \frac{Pl}{\sigma_u t b^2} 6\left[\left(\frac{l}{b}\right)\left(\frac{a}{b}\right) h\left(\frac{a}{b}\right)\right] \quad (12)$$

The term within square brackets is the dimensionless compliance, which, even in this case, depends on beam slenderness and crack depth. Some linear load–CMOD diagrams are shown in Fig. 3 for $l/b = 4$ and varying crack depth a/b.

The set of crack propagation points with s = constant and varying crack depth represents a virtual process even in this case. When the crack grows, the product on the right-hand side of Equation 12 always increases, the compliance increase prevailing over the critical load decrease for each value of a/b. The P–w_1 curve always presents a negative derivative, and the CMOD increases even when both load and deflection decrease ($dP/d\delta > 0$) in the catastrophic P–δ branch. If the CMOD is controlled, i.e. if w_1 increases monotonically without jumping, it would be possible to move along the virtual P–δ path with a positive slope.

The set of ultimate strength points for varying crack depth is represented by the thick line in Fig. 3, which intersects the crack propagation curves with $s \leqslant s_0 = 0.50$ (see also Figs 1 and 2).

A fracture model similar to that described in the present section was proposed by Jenq and Shah [10,11].

4. TESTING EQUIPMENT AND EXPERIMENTAL MEASUREMENTS

The experimental study was carried out using a testing apparatus whose plan is outlined in Fig. 4. The concrete beams, tested utilizing three-point bending, were placed in a steel frame appropriately stiffened by ribs in the lower part. The reaction-moving steel beam was mounted below the specimen, and the loading resulted from a fixed steel element that acted against the upper beam of the testing machine.

The actuator that moved the lower reaction beam was formed by a double-acting hydraulic jack with a maximum load of 20 kN, monitored by a Moog servo-valve monostage with a nominal flow of 1 l min^{-1}.

The driving signal reached the servoactuator from a PID regulator. The reference signal, generated by a personal computer by means of a D/A converter with a

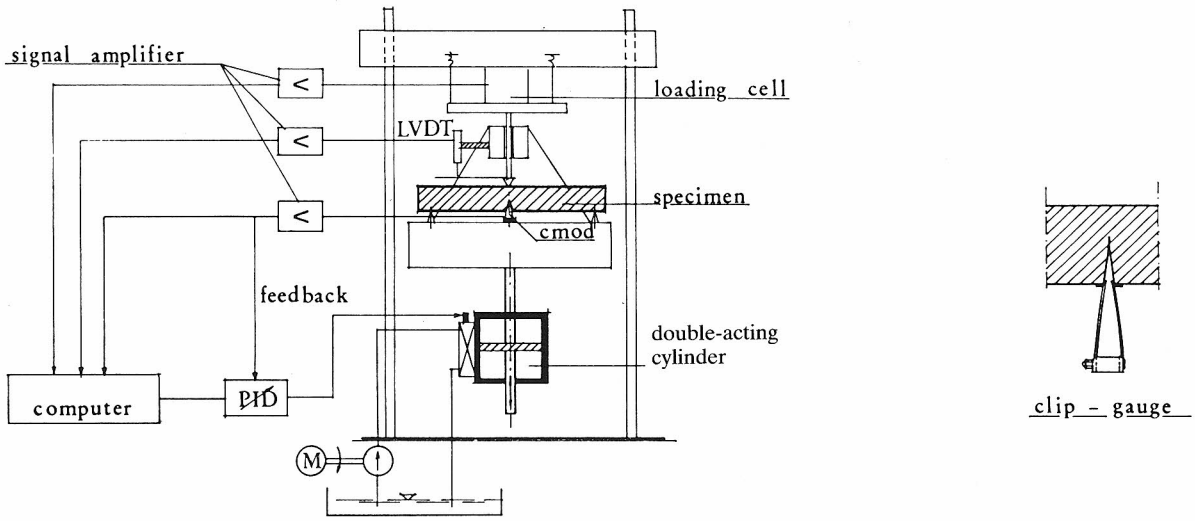

Fig. 4 Oleodynamic block diagram.

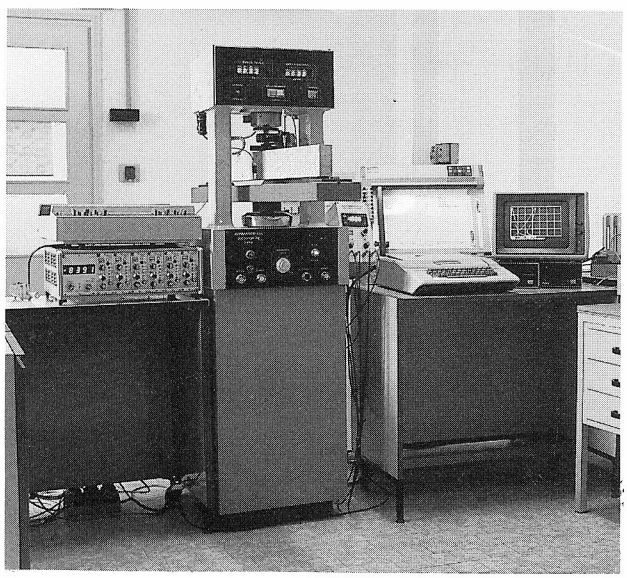

Fig. 5 Testing system.

resolution of 12 bits, was compared to the feedback signal which was appropriately amplified, and was derived from a conventional cantilever-type clip-gauge (TML model UB5A). The resulting feedback quantity was the CMOD which was, therefore, imposed on the specimen with a constant increase with time (equal to 0.12 μm sec^{-1}).

The survey of loads and deflections in the midspan was carried out by means of a load cell (HBM model C4) and an inductive displacement transductor (LVDT, HBM model W5TK), respectively. A view of the testing system is shown in Fig. 5.

5. EXPERIMENTAL RESULTS

The material investigated experimentally was a high-strength concrete [12,13]. The mix proportions by weight were aggregate/sand/cement/water = 2.0/1.5/1.0/0.33. The mechanical properties are reported in Table 1.

The sizes of the beam specimen were constant in all cases: thickness t = 50 mm, height b = 100 mm, length l = 400 mm. The only parameter which was varied was the initial crack length: a_0 = 5, 10, 20, 30, 40, 50, 60, 70, 80 mm. In each case two specimens were tested, and the results for the total number (18) of specimens together with the average values are reported in Table 2.

The load–deflection and load–CMOD experimental diagrams are plotted in Figs 6 and 7. The mechanical response of the specimens with deep cracks appears stable (Fig. 6). Both load–deflection and load–CMOD curves show the same shape with a softening branch of negative slope. By decreasing the relative crack depth

Table 1 Mechanical properties of concrete

Compressive strength	123.5 N mm^{-2}
Tensile (split) strength	9.02 N mm^{-2}
Young's modulus	44145 N mm^{-2}

Table 2 Results of tests

Relative crack depth, a_0/b	Max. load (N)		
	Test 1	Test 2	Mean
0.05	7391.83	7463.00	7477.42
0.1	7543.79	7650.20	7597.00
0.2	5171.15	5307.65	5239.40
0.3	3668.13	4591.08	4130.01
0.4	3078.13	3205.00	3141.57
0.5	1832.22	1940.30	1886.26
0.6	1404.70	1491.20	1447.95
0.7	784.80	961.38	873.09
0.8	323.73	392.40	358.07

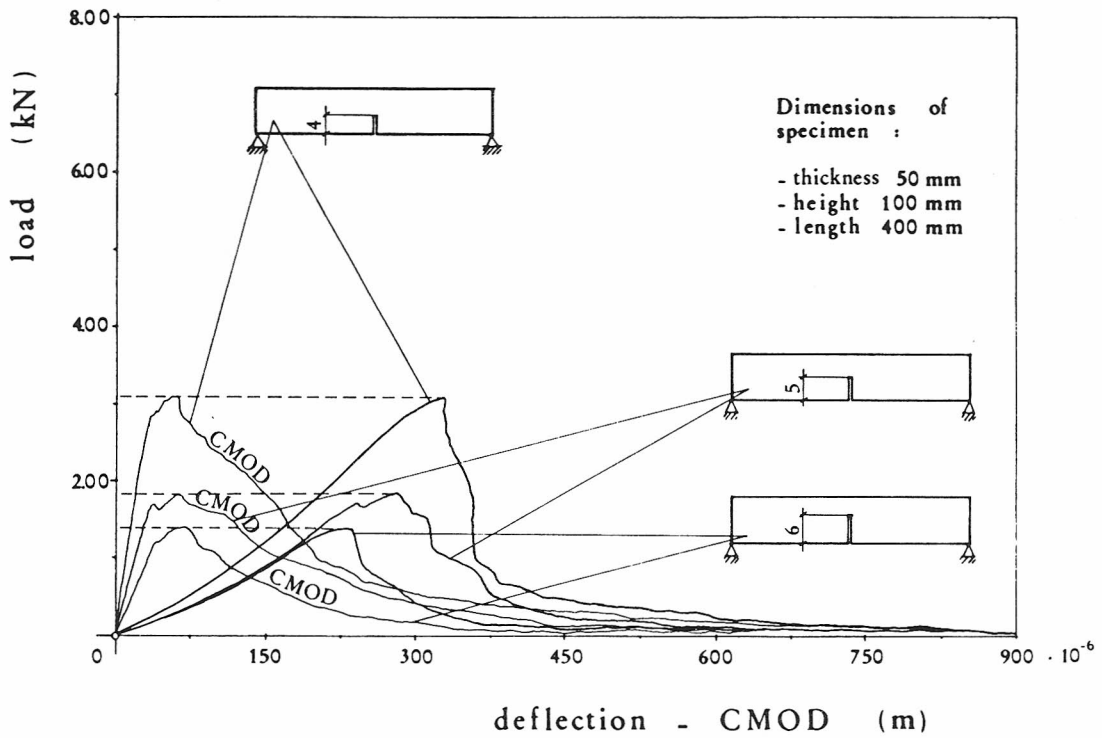

Fig. 6 Experimental load–deflection and load–CMOD diagrams ($a_0/b = 0.4, 0.5, 0.6$). Dimensions of specimen: thickness 50 mm, height 100 mm, length 400 mm.

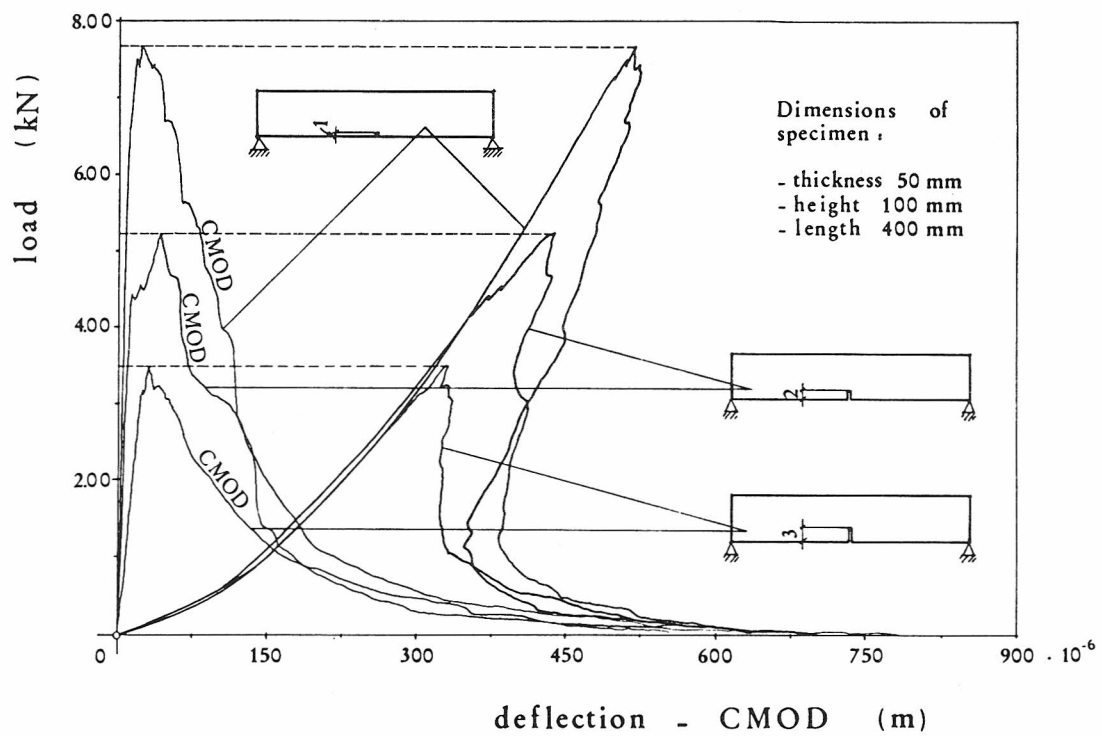

Fig. 7 Experimental load–deflection and load–CMOD diagrams ($a_0/b = 0.1, 0.2, 0.3$).

such a branch becomes steeper with an increase in the brittleness of the system. At the same time, obviously, loading capacity and stiffness increase.

The specimens with shallow cracks (Fig. 7), on the contrary, present a very unstable behaviour. Whereas the load–CMOD curves have a softening tail with negative slope, the load–deflection curves are characterized by a snap-back softening instability with a softening branch of partial positive slope. More precisely, the case $a_0 = 30$ mm shows an almost vertical drop in the loading capacity when the maximum load is achieved. This experimental finding confirms the theoretical result in Fig. 2. In fact, the relative crack depth $a_0/b = 0.3$ is the critical condition between stability and instability for deflection-controlled loading processes. If the loading process had been deflection-controlled, then, once the bifurcation point of the loading path was reached, the load would have presented a negative jump down to the lower softening branch with a negative slope. Therefore, it is evident that, although the process is unstable in nature, it can develop in a stable manner if CMOD-controlled.

All the diagrams in Figs 6 and 7 converge towards the same asymptotic tail, the limit situation being independent of the initial crack length.

The previous theoretical and experimental analyses emphasize that the (brittle or ductile) structural behaviour is connected with a geometrical feature, as is the case for the crack depth. More generally, all the geometrical features of the specimen influence the global brittleness (or ductility), and particularly slenderness and size-scale. This is supported and demonstrated by a very extensive experimental investigation carried out by the present authors.

The snap-back instability is also revealed for rocks [14] and mortar [15]. On the other hand, the snap-back softening instability can be interpreted as an LEFM instability and predicted by the well-known condition $K_I = K_{IC}$. The values of K_{IC}, obtained from Equation 1, are plotted in Fig. 8 against the relative crack depth. They appear nearly constant for $a_0/b \lesssim 0.4$, and then decrease with the crack depth. The fictitious K_{IC} values related to crack depths $a_0/b = 0.05$, 0.7 and 0.8 are also reported. They present values much lower than the others, since in this case the ultimate tensile strength collapse at the ligament clearly precedes the LEFM instability (Figs 1 and 2, $s = 0.52$).

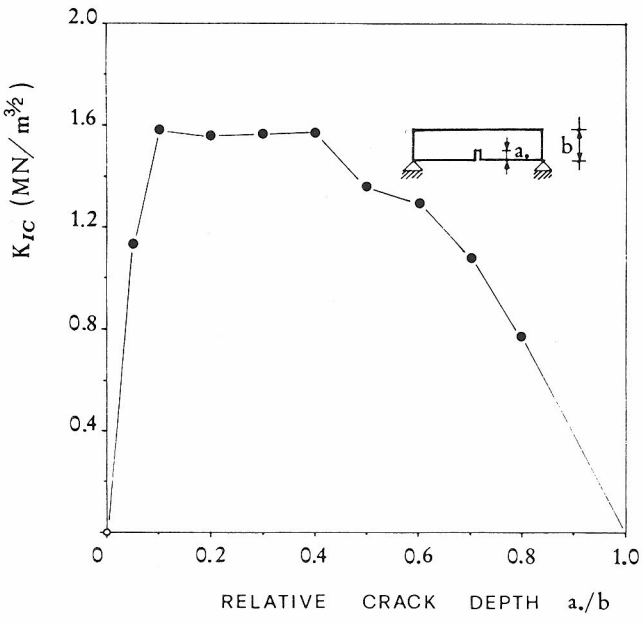

Fig. 8 Fictitious fracture toughness against relative crack depth.

6. CONCLUSIONS

1. Up to the relative crack depth $a_0/b \simeq 0.4$ the maximum load is predicted by LEFM and a snap-back instability is detected.

2. For $a_0/b \gtrsim 0.4$ the failure is of a mixed type between the ultimate strength at the ligament and the LEFM instability (Fig. 1).

3. The geometrical features of the specimen influence the mechanical response, so that the same material can appear brittle as well as ductile. Such features include, for example, relative crack depth, beam slenderness and structure size-scale.

REFERENCES

1. Carpinteri, A., 'Size effects on the brittleness of concrete structures' (in Italian), in Proceedings of AITEC Conference, Parma, October 1985 (1985) pp. 109–123.
2. Carpinteri, A. and Fanelli, M., 'Numerical analysis of the catastrophical softening behaviour in brittle structures', in Proceedings of 4th International Conference on Numerical Methods in Fracture Mechanics, San Antonio, Texas, March 1987 (Pineridge Press, 1987) pp. 369–386.
3. Carpinteri, A., 'Interpretation of the Griffith instability as a bifurcation of the global equilibrium', in Proceedings of NATO Advanced Research Workshop on Application of Fracture Mechanics to Cementitious Composites, Northwestern University, September 1984, edited by S. P. Shah (Nijhoff, 1985) pp. 287–316.
4. *Idem*, 'Limit analysis for elastic-softening structures: scale and slenderness influence on the global brittleness', in 'Structure and Crack Propagation in Brittle Matrix Composite Materials', Proceedings of Euromech Colloquium No. 204, Jablonna, November 1985, edited by A. M. Brandt (Elsevier Applied Science, 1986) pp. 497–508.
5. 'Standard Method of Test for Plane Strain Fracture Toughness of Metallic Materials', E 399-74 (ASTM).
6. Carpinteri, A., 'Size effect in fracture toughness testing: a dimensional analysis approach', in Proceedings of International Conference on Analytical and Experimental Fracture Mechanics, Roma, June 1980, edited by G. C. Sih and M. Mirabile (Sijthoff & Noordhoff, 1981) pp. 785–797.
7. Carpinteri, A., Marega, C. and Savadori, A., 'Size effects and ductile–brittle transition of polypropylene', *J. Mater. Sci.*, **21** (1986) 4173–4178.

8. Tada, H., Paris, P. and Irwin, G., 'The Stress Analysis of Cracks Handbook' (Del Research Corporation, St Louis, Missouri, 1963) p. 2.16.
9. Berry, J. P., 'Some kinetic considerations of the Griffith criterion for fracture', *J. Mech. Phys. Solids* **8** (1960) 194–216.
10. Jenq, Y. S. and Shah, S. P., 'A two parameter fracture model for concrete', *J. Engng Mech. ASCE*, **111** (1985) 1227–1241.
11. *Idem*, 'A fracture toughness criterion for concrete', *ibid.* in press.
12. Biolzi, L. and Tognon, G., 'Sulla meccanica della frattura dei calcestruzzi ad alta ed altissima resistenza', *Atti IMTA* (Oct. 1984).
13. *Idem*, 'Strain rate effect on crack propagation in concrete', *J. Theor. Appl. Fract. Mech.* **7**(3) (1987) pp. 200–206.
14. Fairhurst, C., Hudson, J. A. and Brown, E. T., 'Optimizing the control of rock failure in servo-controlled laboratory tests', *Rock Mechan.* **3** (1971) 217–224.
15. Rokugo, K., Ohno, S. and Koyanagi, W., 'Automatical measuring system of load–displacement curves including post-failure region of concrete specimens', in Proceedings of Conference on Fracture Toughness and Fracture Energy of Concrete, Lausanne, October 1985, edited by F. H. Wittmann (Elsevier Science, 1986) pp. 403–411.